JOURNAL OF SPACECRAFT AND ROCKETS
Vol. 30, No. 1, January–February 1993

Effect of Nose Shape on Three-Dimensional Streamlines and Heating Rates

Basil Hassan* and Fred R. DeJarnette†
North Carolina State University, Raleigh, North Carolina 27695
and
E. Vincent Zoby‡
NASA Langley Research Center, Hampton, Virginia 23681

A new method for calculating the three-dimensional inviscid surface streamlines and streamline metrics using Cartesian coordinates and time as the independent variable of integration has been developed. The technique calculates the streamline from a specified point on the body to a point near the stagnation point by using a prescribed pressure distribution in the Euler equations. The differential equations, which are singular at the stagnation point, are of the two-point boundary-value-problem type. Laminar heating rates are calculated using the axisymmetric analog concept for three-dimensional boundary layers and approximate solutions to the axisymmetric boundary-layer equations. Results for elliptic conic forebody geometries indicate that the location of the point of maximum heating depends on the angle of attack of the conic and the type of conic in the plane of symmetry. This location is in general different from the stagnation point. The new method was found to give smooth predictions of heat transfer in the nose region where previous methods gave oscillatory results.

Nomenclature

a	= conic section principal axis in x direction
b	= conic section principal axis in y direction
b_y	= conic section parameter, b^2/a^2
$\mathcal{C}$	= conic section parameter, b^2/c^2
C_p	= coefficient of pressure
c	= conic section principal axis in z direction
$\hat{e}_s, \hat{e}_n, \hat{e}_\beta$	= unit vectors in streamline coordinate system
F	= equation of surface in Cartesian coordinates (Monge's form)
f	= equation of surface in Cartesian coordinates
h	= streamline metric, normalized by R_{n_y}
I	= heating rate integral defined by Eq. (62)
$\hat{i}, \hat{j}, \hat{k}$	= unit vectors in Cartesian coordinate system
M	= Mach number
n	= normal coordinate direction, normalized by R_{n_y}
p	= static pressure, normalized by $\rho_\infty V_\infty^2$
q	= heat transfer rate
R_{n_y}	= nose radius of curvature in x-y plane of symmetry
r	= cylindrical coordinate, normalized by R_{n_y}
s	= streamline coordinate direction, normalized by R_{n_y}
t	= time variable, normalized by V_∞/R_{n_y}
u, v, w	= Cartesian velocity components, normalized by V_∞
V	= velocity vector, normalized by V_∞
x, y, z	= Cartesian coordinates, normalized by R_{n_y}
α	= angle of attack, deg
β	= coordinate normal to streamline on body surface
γ	= ratio of specific heats
Δt	= time step, normalized by V_∞/R_{n_y}
ϵ	= y coordinate measured from stagnation point, normalized by R_{n_y}
ρ	= density, normalized by ρ_∞
ϕ	= cylindrical coordinate, deg
Ψ	= body angle defined by Eq. (18), deg

Subscripts

d	= value at initial downstream point
i	= spatial step
n	= value at nose point of surface
o	= value at point nearest stagnation point
ref	= reference value
stag	= value at stagnation point
wall	= value at the wall
y	= derivative with respect to y
z	= derivative with respect to z
β	= derivative with respect to β
∞	= freestream value

Superscripts

n	= iteration level
$'$	= first derivative with respect to time

Received Nov. 30, 1991; presented as Paper 91-5032 at the AIAA 3rd International Aerospace Planes Conference, Orlando, FL, Dec. 3-5, 1991; revision received May 7, 1992; accepted for publication June 30, 1992.

*Research Assistant, Mechanical and Aerospace Engineering. Student Member AIAA.

†Professor, Mechanical and Aerospace Engineering. Associate Fellow AIAA.

‡Aero-Space Technologist, Aerothermodynamics Branch, Space Systems Division. Associate Fellow AIAA.

Introduction

THE renewed interest in the area of hypersonic aerodynamics has brought forth the need for low-cost, approximate methods to be used in the prediction of surface heating rates. Engineering codes of this type are used in preliminary vehicle design studies and spacecraft trajectory analysis applications. These methods provide multiple parametric studies where the use of more complex computational fluid dynamics (CFD) codes is impractical.

The computational effort required for the solution of the three-dimensional boundary-layer equations can in general be quite extensive. However, significant reductions can be made by using the approximate "axisymmetric analog" concept[1] where the three-dimensional boundary-layer equations are written in streamline coordinates and the crossflow velocity is assumed to be negligible. The three-dimensional equations are then identical to the axisymmetric form of the equations at 0 deg angle of attack provided two assumptions are made: the

streamline distance is interpreted to be the surface distance along an "equivalent body," and the equivalent body radius is represented by the streamline metric.

Two methods have been used for solving the streamline equations. The first way is to determine the streamlines from a prescribed pressure distribution on the surface of the body in question. Both first and second derivatives of the pressure are required to obtain the streamline metric, which is a measure of the convergence or divergence of adjacent streamlines. An alternate method employs inviscid velocity components to determine the streamlines. Typically, these velocity components are obtained from a CFD solution of the Euler equations. First derivatives of the velocity components are needed for this method to determine the streamline metric.

An approximate method was developed in the early 1970s by DeJarnette and Hamilton.[2] Versions of this code, known today as AEROHEAT or NHEAT, calculate the laminar and turbulent surface heating rates on three-dimensional configurations at an angle of attack using the axisymmetric analog concept. Surface streamlines are traced from a point in the stagnation region using a space marching technique and a known surface pressure distribution. One of the undesirable features of this procedure is that the streamline required to go through a specified point downstream must be determined iteratively.

The streamline equations are singular at the stagnation point where the velocity is zero. Therefore, integration of the necessary equations must begin a finite distance away from the stagnation point and result in heating-rate oscillations in this region. Thus, initial conditions at this point must be derived from approximate relations which were found to be inaccurate. Another difficulty encountered is integrating through the nose point using cylindrical coordinates where the radius goes to zero and the ϕ coordinate is discontinuous. At angle of attack, particularly for long slender bodies, streamlines tend to cluster near the leeward plane of symmetry. As a result of this characteristic, a uniform heating distribution is not provided in regions of interest or at specific user supplied points downstream without multiple runs of the code.

Other investigations have made use of pressure distributions to determine the streamline paths and metric coefficients. Leigh and Ross[3] investigated three different methods for solving the streamline geometry on sphere cones at an angle of attack: geodesic, steepest-descent, and pressure. They employed both the modified Newtonian pressure distribution and an analytic sine-variation method due to Berman.[4] The numerical integrations performed were of the shooting-method type. Vaglio-Laurin[5] also employed a shooting method by tracing out streamlines from points enclosing the stagnation point by determining initial values of the velocity direction on a curve adjacent to the stagnation line. Vollmers[6] obtained the streamline patterns in cylindrical coordinates by using a shooting technique to solve for the angle between the streamline and a line of symmetry. An initial value of the angle was assumed at a point downstream and the first-order ordinary differential equation was numerically integrated upstream toward the stagnation point.

Hamilton et al.[7] proposed several new ideas to circumvent many of the aforementioned problems. Instead of using the pressure technique, an approach employing the inviscid surface velocity components was used since only first derivatives of the velocity components are required to calculate the streamlines and metric. The HALIS code,[8] a three-dimensional time-dependent solution of the Euler equations, is used to obtain the inviscid solution and is run on a vector processing machine. The first derivatives of the surface velocity components were generated numerically. Similar investigations using inviscid flowfield solutions to calculate the streamlines have been performed by other investigators.[9-12]

Typically, small spatial step sizes are required when integrating near the nose point or stagnation point due to the indeterminacy of the streamline equations. Hamilton introduced a "time-like" variable of integration τ defined by

$$\frac{ds}{d\tau} = Vr$$

where s is the surface distance along the streamline, V the velocity, and r the body radius. One can begin at some point just downstream of the stagnation point at $\tau = 0$ and integrate toward the stagnation point. The actual stagnation point ($\tau \rightarrow -\infty$) cannot be computed numerically since $V = 0$ there, but one can get as close as desired. Similarly, when computing the leeward plane of symmetry streamline, τ approaches $+\infty$ at the nose point. Consequently, a streamline that passes very close to the nose point and the leeward plane of symmetry is computed instead of using the time-like integration. Finally, spatial integrations are used in regions of nonsingularities. However, the major drawback of the method[7] is the computational effort needed to compute the inviscid solution. The extensive CPU time necessary to execute HALIS is an unattractive option for fast, approximate methods.

The method of solution for determining the streamlines differs for the velocity and pressure methods. The streamline equations employing the velocity components are first-order differential equations and can be solved using a marching procedure. The initial conditions to determine a streamline that passes through a prescribed downstream point are unknown for a marching procedure. However, the streamline and metric equations using the pressure are second-order differential equations and are of the two-point boundary-value-problem type.

This paper develops a new method for the calculation of three-dimensional surface streamlines and metrics and is based on the work of Ref. 13. Employing the pressure technique eliminates the need of using a full flowfield solver to determine the inviscid velocity components and therefore reduces the computational time. The modified Newtonian pressure distribution is used in this investigation for simplicity only to illustrate the use of this method, although a more accurate pressure distribution can be used instead. In addition, the use of Cartesian coordinates instead of cylindrical or spherical coordinates eliminates the problems at the nose point. A significant feature of the method is that time replaces streamline distance as the independent variable of integration. An investigation of the effect of the forebody geometry on laminar heating rates is made using this new method.

Streamline Equations

To calculate the streamline geometry, begin with the Euler equations that govern the flow of an inviscid, nonconducting gas:

$$\frac{DV}{Dt} = -\frac{\nabla p}{\rho} \tag{1}$$

where D/Dt is a derivative along a streamline. Nondimensional variables will be employed such that all length scales will be normalized by R_{n_y}, the nose radius of curvature in the x-y plane; the velocity by V_∞; the pressure by $\rho_\infty V_\infty^2$; and the density by ρ_∞. In Cartesian coordinates (see Fig. 1), the velocity is given by

$$V = V\hat{e}_s = u\hat{i} + v\hat{j} + w\hat{k} = \frac{Dx}{Dt}\hat{i} + \frac{Dy}{Dt}\hat{j} + \frac{Dz}{Dt}\hat{k} \tag{2}$$

and the equation of the surface is represented by

$$F(x,y,z) = f(y,z) - x = 0 \tag{3}$$

It should be noted that the equation of the surface may not always be expressed as a single variable explicitly in terms of the other two independent variables. However, there is no loss in generality in using $x = f(y,z)$ since derivatives of f can be

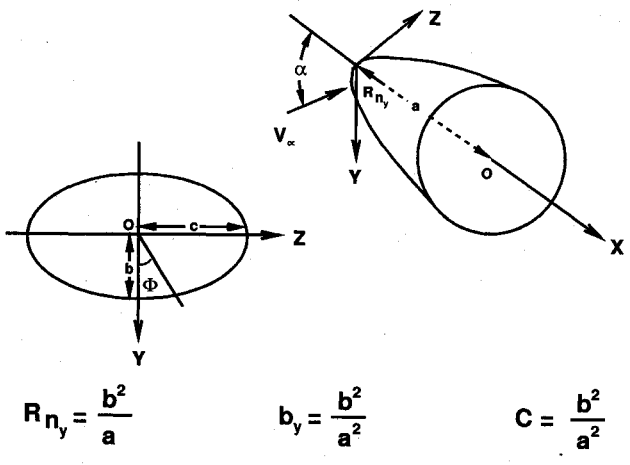

Fig. 1 Elliptic conic forebody geometry and coordinate system.

expressed as functions of F, i.e.,

$$f_y = -\frac{F_y}{F_x}, \qquad f_z = -\frac{F_z}{F_x}$$

It is advantageous to use y and z as independent variables on the surface since all derivatives of f are either finite or zero at the nose point. From Eq. (3), the first and second derivatives of x can be determined in terms of y, z, and their derivatives with respect to time.

$$\frac{Dx}{Dt} = u = f_y\frac{Dy}{Dt} + f_z\frac{Dz}{Dt} \tag{4}$$

$$\frac{D^2x}{Dt^2} = \frac{Du}{Dt} = f_y\frac{D^2y}{Dt^2} + f_z\frac{D^2z}{Dt^2} + f_{yy}\left[\frac{Dy}{Dt}\right]^2 + 2f_{yz}\left[\frac{Dy}{Dt}\right]\left[\frac{Dz}{Dt}\right] + f_{zz}\left[\frac{Dz}{Dt}\right]^2 \tag{5}$$

The pressure is considered as a function of y, z, and n (normal distance). Each component of Eq. (1) can be written in terms of the preceding variables where $n = 0$ on the surface.

$$\frac{D^2x}{Dt^2} = -\frac{n_x}{\rho}\frac{\partial p}{\partial n} \tag{6}$$

$$\frac{D^2y}{Dt^2} = -\frac{1}{\rho}\left[\frac{\partial p}{\partial y} + n_y\frac{\partial p}{\partial n}\right] \tag{7}$$

$$\frac{D^2z}{Dt^2} = -\frac{1}{\rho}\left[\frac{\partial p}{\partial z} + n_z\frac{\partial p}{\partial n}\right] \tag{8}$$

The body normal (outer) is defined by

$$\hat{e}_n = \frac{\nabla F}{|\nabla F|} = n_x\hat{i} + n_y\hat{j} + n_z\hat{k} = \frac{-\hat{i} + f_y\hat{j} + f_z\hat{k}}{\sqrt{1 + f_y^2 + f_z^2}} \tag{9}$$

The set of Eqs. (6-8) can be reduced to two equations on the surface by substituting for D^2x/Dt^2 from Eq. (5) and $\partial p/\partial n$ from Eq. (6) into Eqs. (7) and (8). The result is

$$\frac{D^2y}{Dt^2} = -\frac{f_yf_{yy}}{|\nabla F|^2}\left[\frac{Dy}{Dt}\right]^2 - \frac{2f_yf_{yz}}{|\nabla F|^2}\left[\frac{Dy}{Dt}\right]\left[\frac{Dz}{Dt}\right] - \frac{f_yf_{zz}}{|\nabla F|^2}\left[\frac{Dz}{Dt}\right]^2 + \frac{1}{\rho|\nabla F|^2}\left[f_yf_z\frac{\partial p}{\partial z} - (1+f_z^2)\frac{\partial p}{\partial y}\right] \tag{10}$$

$$\frac{D^2z}{Dt^2} = -\frac{f_zf_{yy}}{|\nabla F|^2}\left[\frac{Dy}{Dt}\right]^2 - \frac{2f_zf_{yz}}{|\nabla F|^2}\left[\frac{Dy}{Dt}\right]\left[\frac{Dz}{Dt}\right] - \frac{f_zf_{zz}}{|\nabla F|^2}\left[\frac{Dz}{Dt}\right]^2 + \frac{1}{\rho|\nabla F|^2}\left[f_yf_z\frac{\partial p}{\partial y} - (1+f_y^2)\frac{\partial p}{\partial z}\right] \tag{11}$$

where

$$|\nabla F|^2 = 1 + f_y^2 + f_z^2 \tag{12}$$

It is noted that Eqs. (10) and (11) are second-order, nonlinear differential equations in the coordinates y and z and involve first and second derivatives of the body geometry and first derivatives of the pressure on the surface.

To work with dependent variables that go to zero at the stagnation point, employ the following change of variable:

$$\epsilon \equiv y - y_{\text{stag}} \tag{13}$$

and rewrite Eqs. (10) and (11) as

$$\frac{D^2\epsilon}{Dt^2} = A, \qquad \text{and} \qquad \frac{D^2z}{Dt^2} = B \tag{14}$$

where A and B are defined by the right sides of Eqs. (10) and (11). Also define

$$\frac{D\epsilon}{Dt} \equiv \epsilon', \quad \text{and} \quad \frac{Dz}{Dt} \equiv z' \tag{15}$$

Since the differential equations are second order, two boundary conditions are needed to obtain a solution, one at the selected downstream point and one near the stagnation point. The downstream point is chosen at time $t = 0$, thus the stagnation point is located at time $t \to -\infty$ since $V = 0$ at the stagnation point. This result follows from the definition of the time variable used:

$$\frac{Ds}{Dt} = V \tag{16}$$

Use of time instead of distance s as the independent variable allows the stagnation region to be magnified relative to time. However, to integrate to $t = -\infty$ is numerically impossible. As a result, integration to a point very close to the stagnation point will be performed. The boundary condition at that point must be determined carefully since the coordinates are not known a priori.

Surface Pressure Distribution

The modified Newtonian pressure distribution will be assumed on the surface of the geometries considered to illustrate the streamline and metric calculation method, although any other analytic pressure distribution could be employed. The nondimensional pressure distribution is governed by the following relation:

$$p = p_\infty + \tfrac{1}{2}C_{p_{\text{stag}}}\sin^2\Psi \tag{17}$$

where

$$\sin\Psi = -\hat{V}_\infty \cdot \hat{e}_n \tag{18}$$

$$\hat{V}_\infty = (\cos\alpha\,\hat{i} - \sin\alpha\,\hat{j}) \tag{19}$$

The stagnation point is located at $\Psi = \pi/2$. For the shadowed region, where $\Psi < 0$, the pressure is assumed to be equal to the freestream value.

An alternate pressure distribution developed by Love et al.[14] involving the use of a "sin²-deficiency method" was also considered for the calculation of heating rates on spherically blunted wide angle cones at 0 deg angle of attack where the

sonic point occurs at the base. Results employing this pressure distribution are presented in Ref. 13.

Elliptic Conic Forebody Geometry

An elliptic conic forebody geometry was considered in this investigation. The equation for this geometry is given by the following (see Fig. 1):

$$y^2 + \mathcal{C}z^2 = 2R_{n_y}x - b_y x^2 \tag{20}$$

The nose radius of curvature in the x-y plane of symmetry R_{n_y} is

$$R_{n_y} = b^2/a$$

Solve for x and nondimensionalize all lengths by R_{n_y} to obtain

$$x = f(y,z) = \frac{1}{b_y}\left[(1 - \sqrt{1 - b_y(y^2 + \mathcal{C}z^2)}\right], \qquad b_y \neq 0 \tag{21}$$

and

$$x = f(y,z) = \frac{y^2 + \mathcal{C}z^2}{2}, \qquad b_y = 0 \tag{22}$$

where

$$b_y = \frac{b^2}{a^2} \qquad \text{and} \qquad \mathcal{C} = \frac{b^2}{c^2}$$

The parameters a, b, and c are the principal axes of the elliptic conic in the x, y, and z coordinate directions, respectively. All of the conic sections with elliptical cross sections can be described by this equation. An ellipsoid results when b_y is positive, a hyperboloid when b_y is negative, and a paraboloid when b_y is zero. A spherical geometry is the axisymmetric case of the ellipsoid where $b_y = \mathcal{C} = 1$.

The expression for sin Ψ for an elliptic conic geometry using Eqs. (9), (18), and (19) is

$$\sin\Psi = \frac{\cos\alpha\sqrt{1 - b_y(y^2 + \mathcal{C}z^2)} + y\sin\alpha}{\sqrt{1 + (1 - b_y)y^2 + \mathcal{C}(\mathcal{C} - b_y)z^2}} \tag{23}$$

Stagnation Region Boundary Conditions

To determine boundary conditions for the stagnation region, a limiting form of the streamline equations is derived. The intent is to reduce Eqs. (10) and (11) to forms accurate to second order terms. The terms on the right sides of Eqs. (10) and (11) are expanded by a Taylor series in four independent variables: ϵ, z, ϵ', and z'.

The pressure is dependent on ϵ and z only. It is noted that the first derivatives of the pressure are zero at the stagnation point. Then retaining only the terms up to second order in ϵ and z results in the following expressions for the pressure gradients:

$$\frac{\partial p}{\partial y} \approx \left(\frac{\partial^2 p}{\partial y^2}\right)_{\text{stag}} \epsilon + \frac{1}{2}\left(\frac{\partial^3 p}{\partial y^3}\right)_{\text{stag}} \epsilon^2 + \frac{1}{2}\left(\frac{\partial^3 p}{\partial y\,\partial z^2}\right)_{\text{stag}} z^2 \tag{24}$$

and

$$\frac{\partial p}{\partial z} \approx \left(\frac{\partial^2 p}{\partial z^2}\right)_{\text{stag}} z + \left(\frac{\partial^3 p}{\partial y\,\partial z^2}\right)_{\text{stag}} \epsilon z \tag{25}$$

Expansions of the respective coefficients of the pressure gradient and velocity terms are also performed in a similar fashion. Substitute all terms into Eq. (10) to get

$$\frac{\mathrm{D}^2\epsilon}{\mathrm{D}t^2} \approx a_y\epsilon + a_{yy}\epsilon^2 + a_{zz}z^2 + a_{y'y'}\epsilon'^2 + a_{z'z'}z'^2 \tag{26}$$

Similarly, Eq. (11) reduces to

$$\frac{\mathrm{D}^2 z}{\mathrm{D}t^2} \approx a_z z + a_{yz}\epsilon z \tag{27}$$

where the coefficients of ϵ, z, ϵ', and z' are functions of $C_{p\text{stag}}$, ρ_{stag}, α, b_y, and $\mathcal{C}$.

Equations (24–27) can be integrated analytically to second-order accuracy for the region very near the stagnation point. Approximate expressions for ϵ and z can be determined subject to the following boundary conditions:

$$\epsilon(t \to -\infty) = 0, \qquad \epsilon(t = t_o) = \epsilon_o$$

and

$$z(t \to -\infty) = 0, \qquad z(t = t_o) = z_o$$

The location of the point (ϵ_o, z_o) is not known initially and is determined by the solution procedure.

First-order solutions to the homogeneous parts of Eqs. (26) and (27) are

$$\epsilon \approx \epsilon_o \exp\left[\sqrt{a_y}(t - t_o)\right] \tag{28}$$

and

$$z \approx z_o \exp\left[\sqrt{a_z}(t - t_o)\right] \tag{29}$$

Substitute the homogeneous solutions into the nonlinear terms of Eqs. (26) and (27) and solve the resulting differential equations by the method of variation of parameters to get

$$\epsilon \approx \left(\epsilon_o - \frac{\tilde{B}}{3\tilde{A}}\epsilon_o^2 - \frac{\tilde{C}}{4\tilde{D} - \tilde{A}}z_o^2\right)\exp\left[\sqrt{\tilde{A}}\,(t - t_o)\right] + \frac{\tilde{B}}{3\tilde{A}}\epsilon_o^2 \exp\left[2\sqrt{\tilde{A}}\,(t - t_o)\right] + \frac{\tilde{C}}{4\tilde{D} - \tilde{A}}z_o^2 \exp\left[2\sqrt{\tilde{D}}(t - t_o)\right] \tag{30}$$

and

$$z \approx \left(z_o - \frac{\tilde{E}}{2\sqrt{\tilde{A}\tilde{D}} + \tilde{A}}\epsilon_o z_o\right)\exp\left[\sqrt{\tilde{D}}\,(t - t_o)\right] + \frac{\tilde{E}}{2\sqrt{\tilde{A}\tilde{D}} + \tilde{A}}\epsilon_o z_o \exp\left[(\sqrt{\tilde{A}} + \sqrt{\tilde{D}})\,(t - t_o)\right] \tag{31}$$

where

$$\tilde{A} = a_y, \qquad \tilde{B} = a_{yy} + a_y a_{y'y'}, \qquad \tilde{C} = a_{zz} + a_z a_{z'z'}$$

$$\tilde{D} = a_z, \qquad \tilde{E} = a_{yz}$$

Differentiate Eqs. (30) and (31) to get approximate relations for the ϵ and z components of velocity, respectively, at $t = t_o$:

$$\frac{\mathrm{D}\epsilon}{\mathrm{D}t} \approx \sqrt{\tilde{A}}\,\epsilon_o + \frac{\tilde{B}}{3\sqrt{\tilde{A}}}\epsilon_o^2 + \frac{\tilde{C}}{2\sqrt{\tilde{D}} + \sqrt{\tilde{A}}}\,z_o^2 \tag{32}$$

and

$$\frac{\mathrm{D}z}{\mathrm{D}t} \approx \sqrt{\tilde{D}}\,z_o + \frac{\tilde{E}}{2\sqrt{\tilde{D}} + \sqrt{\tilde{A}}}\,\epsilon_o z_o \tag{33}$$

where Eqs. (32) and (33) will be referred to as the stagnation region boundary conditions for the streamline equations. It is again reiterated that these expressions are only valid near the stagnation point of an elliptic conic forebody geometry.

Solution Procedure

The resulting differential equations, Eqs. (10) and (11), are of the two-point boundary-value-problem type, therefore, a numerical marching procedure toward the stagnation point is not possible. Instead the streamline equations will be solved using a fully implicit, finite difference algorithm. Because of the nonlinearity of the equations, the solution of these equations will require an iterative procedure. Since A and B are

functions of ϵ, z, ϵ', and z', apply a Newton-Raphson quasilinearization technique[15] to obtain

$$\frac{D^2\epsilon}{Dt^2} = \bar{A} + \frac{\partial \bar{A}}{\partial \bar{\epsilon}}(\epsilon - \bar{\epsilon}) + \frac{\partial \bar{A}}{\partial \bar{z}}(z - \bar{z}) + \frac{\partial \bar{A}}{\partial \bar{\epsilon}'}(\epsilon' - \bar{\epsilon}') + \frac{\partial \bar{A}}{\partial \bar{z}'}(z' - \bar{z}') \tag{34}$$

$$\frac{D^2 z}{Dt^2} = \bar{B} + \frac{\partial \bar{B}}{\partial \bar{\epsilon}}(\epsilon - \bar{\epsilon}) + \frac{\partial \bar{B}}{\partial \bar{z}}(z - \bar{z}) + \frac{\partial \bar{B}}{\partial \bar{\epsilon}'}(\epsilon' - \bar{\epsilon}') + \frac{\partial \bar{B}}{\partial \bar{z}'}(z' - \bar{z}') \tag{35}$$

where the barred quantities are evaluated at the previous iteration level. As convergence is achieved, all but the first terms in each equation vanish and the right-hand sides approach their exact values. The partial derivatives of A and B are determined numerically with second-order differencing, although they could be determined analytically for the pressure distributions considered. For example,

$$\frac{\partial A}{\partial \epsilon} = \frac{A(\epsilon + \Delta\epsilon, z, \epsilon', z') - A(\epsilon - \Delta\epsilon, z, \epsilon', z')}{2\Delta\epsilon}$$

where

$$\Delta\epsilon = 0.00001\epsilon, \quad \epsilon > 0$$

$$\Delta\epsilon = 0.00001, \quad \epsilon = 0$$

The numerical derivatives were found to compare with the analytic derivatives to at least four decimal places.

Also, using a second-order central difference approximation to the temporal derivatives, the following finite difference form of the ϵ-streamline equation in block tridiagonal form is obtained from Eq. (34):

$$\begin{aligned}
&\left[1 - \frac{\Delta t}{2}\left(\frac{\partial A}{\partial \epsilon'}\right)_i^n\right]\epsilon_{i-1}^{n+1} - \left[2 + (\Delta t)^2\left(\frac{\partial A}{\partial \epsilon}\right)_i^n\right]\epsilon_i^{n+1} \\
&+ \left[1 + \frac{\Delta t}{2}\left(\frac{\partial A}{\partial \epsilon'}\right)_i^n\right]\epsilon_{i+1}^{n+1} - \left[\frac{\Delta t}{2}\left(\frac{\partial A}{\partial z'}\right)_i^n\right]z_{i-1}^{n+1} \\
&- \left[\frac{\Delta t^2}{2}\left(\frac{\partial A}{\partial z'}\right)_i^n\right]z_{i-1}^{n+1} - \left[\Delta t^2\left(\frac{\partial A}{\partial z}\right)_i^n\right]z_i^{n+1} \\
&+ \left[\frac{\Delta t}{2}\left(\frac{\partial A}{\partial z'}\right)_i^n\right]z_{i+1}^{n+1} \\
&= (\Delta t)^2\left[A_i^n - \left(\frac{\partial A}{\partial \epsilon}\right)_i^n \epsilon_i^n - \left(\frac{\partial A}{\partial z}\right)_i^n z_i^n\right] \\
&+ \frac{\Delta t}{2}\left[\left(\frac{\partial A}{\partial \epsilon'}\right)_i^n (\epsilon_{i+1}^n - \epsilon_{i-1}^n) + \left(\frac{\partial A}{\partial z'}\right)_i^n (z_{i+1}^n - z_{i-1}^n)\right]
\end{aligned} \tag{36}$$

where

$$t = -\sum_i \Delta t_i$$

The subscript i is equal to 1 at the downstream point and increases toward the stagnation point. Typically, 150 to 200 points were used to calculate a streamline.

An equation of similar form is obtained for the z-streamline equation from Eq. (35) by switching ϵ and z and replacing A with B. Equation (36) uses a constant and positive time-step Δt. The use of a constant Δt produced a clustering of the streamline coordinate points near the stagnation point and placed few points in the downstream region. This clustering was necessary for computing accurate heating rates in the stagnation region.

The stagnation region boundary conditions, Eqs. (32) and (33), are quasilinearized where necessary and then differenced about the midpoint of the two points nearest the stagnation point. The resulting finite difference approximations only involve terms of ϵ and z at the two points nearest the stagnation point and form the final two equations in the block tridiagonal matrix.

As discussed, the solution to the streamline equations is iterative and therefore an initial distribution of ϵ and z is required. The stagnation region equations will be applied throughout the region from the stagnation point to the prescribed downstream point to provide an approximate initial distribution. Replace the subscript o with d in Eqs. (30) and (31), where the subscript d represents the selected downstream point where $t_d = 0$ and apply the expressions in the interval

$$t_o < t < 0 = t_d$$

where

$$t_o = -(i\max)\Delta t$$

The resulting expressions were found to give an acceptable initial guess for the streamline solution and to speed convergence considerably. Each iteration gives ϵ_i^{n+1} and z_i^{n+1} for $i = 1$ to $i\max$.

Metric Calculation

Once the streamline geometry has been determined, the streamline metric can be calculated. Let $\boldsymbol{R}_b$ be the position vector for any point on the body.

$$\boldsymbol{R}_b = x\hat{i} + y\hat{j} + z\hat{k} = f(y,z)\hat{i} + y\hat{j} + z\hat{k} \tag{37}$$

and

$$d\boldsymbol{R}_b = (f_y\hat{i} + \hat{j})\,dy + (f_z\hat{i} + \hat{k})\,dz \tag{38}$$

The surface coordinates y and z are now considered to be functions of new independent variables t and β, where β = constant along a streamline. The differential arc lengths along a streamline and in the β direction along the surface are, respectively, $V\,dt$ and $h\,d\beta$. The metric h will be needed later for aerodynamic heating calculations. Then

$$d\boldsymbol{R}_b = V\,dt\hat{e}_s + h\,d\beta\hat{e}_\beta \tag{39}$$

where $\hat{e}_s$ is the unit vector along a streamline, $\hat{e}_\beta$ is the unit vector tangent to the surface but perpendicular to $\hat{e}_s$ and $\hat{e}_n$, and $\hat{e}_n$ is the unit vector normal to the body surface. Equating the right sides of Eqs. (38) and (39) gives

$$V\,dt\hat{e}_s + h\,d\beta\hat{e}_\beta = (f_y\hat{i} + \hat{j})\,dy + (f_z\hat{i} + \hat{k})\,dz \tag{40}$$

Since β is constant along a streamline

$$\left(\frac{\partial}{\partial t}\right)_\beta \equiv \frac{D}{Dt}$$

Equation (40) then gives

$$V\hat{e}_s = (f_y\hat{i} + \hat{j})\frac{Dy}{Dt} + (f_z\hat{i} + \hat{k})\frac{Dz}{Dt} \tag{41}$$

where

$$V^2 = \left(\frac{Dy}{Dt}\right)^2 + \left(f_y\frac{Dy}{Dt} + f_z\frac{Dz}{Dt}\right)^2 + \left(\frac{Dz}{Dt}\right)^2 \tag{42}$$

Therefore take the cross product of Eq. (41) with Eq. (9) to obtain an expression for $\hat{e}_\beta$

$$\hat{e}_\beta = \hat{e}_s \times \hat{e}_n = \frac{1}{V|\nabla F|}\left\{\left(f_z\frac{Dy}{Dt} - f_y\frac{Dz}{Dt}\right)\hat{i}\right.$$

$$-\left[f_z\left(f_y\frac{Dy}{Dt}+f_z\frac{Dz}{Dt}\right)+\frac{Dz}{Dt}\right]\hat{j}$$

$$+\left[f_y\left(f_y\frac{Dy}{Dt}+f_z\frac{Dz}{Dt}\right)+\frac{Dy}{Dt}\right]\hat{k}\Bigg\} \tag{43}$$

Take the dot product of $\hat{j}$ with Eq. (40) to get

$$V\,dt\hat{e}_s\cdot\hat{j}+h\,d\beta\hat{e}_\beta\cdot\hat{j}=dy \tag{44}$$

and the dot product of $\hat{k}$ with Eq. (40) to obtain

$$V\,dt\hat{e}_s\cdot\hat{k}+h\,d\beta\hat{e}_\beta\cdot\hat{k}=dz \tag{45}$$

Combine Eq. (44) with Eq. (45) to eliminate $V\,dt$,

$$h\,d\beta[(\hat{e}_s\cdot\hat{j})(\hat{e}_\beta\cdot\hat{k})-(\hat{e}_s\cdot\hat{k})(\hat{e}_\beta\cdot\hat{j})]$$
$$=\hat{e}_s\cdot\hat{j}\,dz-\hat{e}_s\cdot\hat{k}\,dy \tag{46}$$

Using the unit vectors $\hat{e}_s$ and $\hat{e}_\beta$, it can be shown that

$$(\hat{e}_s\cdot\hat{j})(\hat{e}_\beta\cdot\hat{k})-(\hat{e}_s\cdot\hat{k})(\hat{e}_\beta\cdot\hat{j})=\frac{1}{|\nabla F|} \tag{47}$$

Then Eq. (46) becomes

$$h\,d\beta=\frac{|\nabla F|}{V}\left[\frac{Dy}{Dt}\,dz-\frac{Dz}{Dt}\,dy\right] \tag{48}$$

Since $y=y(t,\beta)$ and $z=z(t,\beta)$, then

$$dy=\frac{Dy}{Dt}\,dt+\frac{\partial y}{\partial\beta}\,d\beta \tag{49}$$

and

$$dz=\frac{Dz}{Dt}\,dt+\frac{\partial z}{\partial\beta}\,d\beta \tag{50}$$

Substitute Eqs. (49) and (50) into Eq. (48), equate the coefficients of $d\beta$, and substitute $d\epsilon$ for dy to obtain the equation for the surface streamline metric h:

$$h=\frac{|\nabla F|}{V}\left[\frac{D\epsilon}{Dt}\frac{\partial z}{\partial\beta}-\frac{Dz}{Dt}\frac{\partial\epsilon}{\partial\beta}\right] \tag{51}$$

where the metric is a measure of the convergence or divergence between adjacent streamlines. The velocity terms $D\epsilon/Dt$ and Dz/Dt are determined using second-order finite differences from the streamline solution, and V follows from Eq. (42). The remaining terms $\partial\epsilon/\partial\beta$ and $\partial z/\partial\beta$ must now be calculated.

Differentiate the streamline equations in Eq. (14) with respect to β to obtain

$$\frac{D^2\epsilon_\beta}{Dt^2}=\frac{\partial A}{\partial\beta}\quad\text{and}\quad\frac{D^2z_\beta}{Dt^2}=\frac{\partial B}{\partial\beta} \tag{52}$$

Boundary conditions at the downstream point are chosen such that for a given axial location, the coordinate β is assigned for a given streamline by its circumferential location, i.e.,

$$y_d=r_d\cos\beta,\qquad z_d=r_d\sin\beta$$

Differentiate the preceding expressions for y_d and z_d with respect to β to obtain

$$\epsilon_{\beta_d}=-r_d\sin\beta+r_{\beta_d}\cos\beta \tag{53}$$

and

$$z_{\beta_d}=r_d\cos\beta+r_{\beta_d}\sin\beta \tag{54}$$

where

$$r_d=\sqrt{\frac{2x_d-b_yx_d^2}{\cos^2\beta+\mathcal{C}\sin^2\beta}} \tag{55}$$

and

$$r_{\beta_d}=\frac{(1-\mathcal{C})r_d\sin\beta\cos\beta}{\cos^2\beta+\mathcal{C}\sin^2\beta} \tag{56}$$

for an elliptic conic forebody. Substitute expressions for y_d and z_d and Eq. (56) into Eqs. (53) and (54) to get

$$\epsilon_{\beta_d}=\epsilon_\beta(t=0)=\frac{-\mathcal{C}z_d}{\cos^2\beta+\mathcal{C}\sin^2\beta}$$

and

$$z_{\beta_d}=z_\beta(t=0)=\frac{y_d}{\cos^2\beta+\mathcal{C}\sin^2\beta}$$

These boundary conditions are not unique and could be determined by any consistent method of assigning β to the streamlines.

Differentiating the stagnation region boundary conditions (32) and (33) with respect to β produces

$$\frac{D\epsilon_\beta}{Dt}\approx\sqrt{\tilde{A}}\,\epsilon_{\beta_o}+\frac{2\tilde{B}}{3\sqrt{\tilde{A}}}\,\epsilon_o\epsilon_{\beta_o}+\frac{2\tilde{C}}{2\sqrt{\tilde{D}}+\sqrt{\tilde{A}}}\,z_oz_{\beta_o} \tag{57}$$

and

$$\frac{Dz_\beta}{Dt}\approx\sqrt{\tilde{D}}\,z_{\beta_o}+\frac{2\tilde{E}}{2\sqrt{\tilde{D}}+\sqrt{\tilde{A}}}\,(z_o\epsilon_{\beta_o}+\epsilon_oz_{\beta_o}) \tag{58}$$

Equations (57) and (58) will serve as the boundary conditions in the stagnation region.

Since A and B are functions of ϵ, z, ϵ', and z', Eqs. (52) are written as

$$\frac{D^2\epsilon_\beta}{Dt^2}=\frac{\partial A}{\partial\epsilon}\,\epsilon_\beta+\frac{\partial A}{\partial z}\,z_\beta+\frac{\partial A}{\partial\epsilon'}\,\epsilon'_\beta+\frac{\partial A}{\partial z'}\,z'_\beta \tag{59}$$

$$\frac{D^2z_\beta}{Dt^2}=\frac{\partial B}{\partial\epsilon}\,\epsilon_\beta+\frac{\partial B}{\partial z}\,z_\beta+\frac{\partial B}{\partial\epsilon'}\,\epsilon'_\beta+\frac{\partial B}{\partial z'}\,z'_\beta \tag{60}$$

The partial derivatives of A and B are the same as those found in the streamline equations and evaluated using the converged values of ϵ and z. By treating ϵ_β and z_β as the dependent variables and employing a second-order central difference approximation to the temporal derivatives, the resulting equations are linear in ϵ_β and z_β. The equations can again be written in block tridiagonal form and only one inversion is necessary due to the linearity. The finite difference form of the equations is identical to the streamline equations (36) except that ϵ_β and z_β are the dependent variables and the right sides equal to zero. Similarly, the finite difference equations for the stagnation region conditions are the same as those for the streamline equations except again with ϵ_β and z_β as the dependent variables and the right sides equal to zero. The algorithm used to solve the equations in block tridiagonal form is given in Ref. 16.

The variation of the metric along a streamline rather than the actual magnitude of the metric is the important parameter in the heating calculations. It will be shown later that only the product hV is needed for the heating calculations.

Aerodynamic Heating Considerations

Once the streamline patterns and metric have been determined for the geometry of interest, the heat transfer rates along the surface can be computed. The basic axisymmetric analog method as outlined in Ref. 1 is employed. The laminar

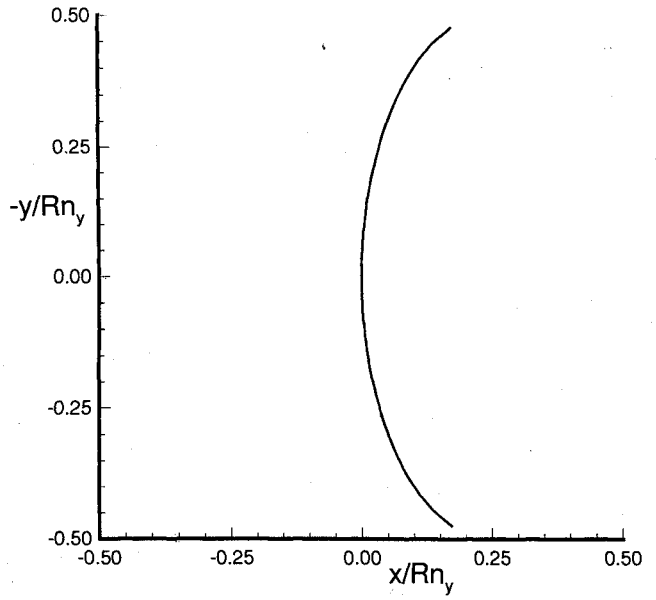

Fig. 2 Plane of symmetry geometry for AFE-like ellipsoid.

heat transfer equation given in Ref. 1 is

$$\frac{q_{\text{wall}}}{q_{\text{wall}_{\text{stag}}}} = \frac{(p/p_{\text{stag}})Vh}{\left[\dfrac{2(G+1)}{V_\infty}\left(\dfrac{\partial V_T}{\partial S_T}\right)_{\text{stag}}\displaystyle\int_0^s \frac{p}{p_{\text{stag}}}\,Vh^2\,\mathrm{D}s\right]^{1/2}} \tag{61}$$

where for the modified Newtonian pressure distribution

$$G = R_T/R_\parallel$$

and

$$\left(\frac{\partial V_T}{\partial S_T}\right)_{\text{stag}} = \frac{1}{R_T}\sqrt{\frac{2(p_{\text{stag}} - p_\infty)}{\rho_{\text{stag}}}}$$

where R_T is the radius of curvature perpendicular to the plane of symmetry and $R_\parallel$ is the radius of curvature parallel to the plane of symmetry, both at the stagnation point. Define the integral in the denominator as

$$I = \int_0^s \frac{p}{p_{\text{stag}}}\,Vh^2\,\mathrm{D}s \tag{62}$$

where I is identically zero at the stagnation point. However, to be consistent with the time integration employed for calculating the streamlines and metric, substitute Eq. (16) into Eq. (62) to get

$$I = \int_{-\infty}^s \frac{p}{p_{\text{stag}}}\,V^2h^2\,\mathrm{D}t \tag{63}$$

Integration of Eq. (63) can be performed using a fourth-order Runge-Kutta method along a streamline by treating the integrand of Eq. (63) as a differential equation, provided an initial value is available. Remembering that integration of the streamline equations is performed over a finite interval of time $t = t_o$ and not to $t = -\infty$, a value for $I(t = t_o)$ must be determined.

From the equation for the metric (51), the product hV can be determined. Approximate relations for ϵ_β and z_β can also be determined by differentiating Eqs. (30) and (31) with respect to β. Substitute the approximate expressions for ϵ_β, z_β, ϵ', z' and first-order Taylor series expansions of the gradient of the body geometry and the pressure term into Eq. (63). Integrating the resulting expression gives an initial condition for the integral that is accurate up to second order. It was necessary to retain the second-order terms to achieve the desired accuracy in the stagnation region. Details of this procedure are given in Ref. 13.

Results and Discussion

Attention has been given lately to blunted hypersonic re-entry vehicles and the levels of heating that occur on these three-dimensional geometries. Vehicles of interest include the National Aero-Space Plane (NASP), the Personnel Launch System (PLS), and the Aeroassist Flight Experiment (AFE). Segments of the forebodies on these and other proposed vehicles can be modeled by simple three-dimensional conics.

In this section, discussion will focus on the trends of the laminar surface heating rates and the streamline geometry. Heat transfer calculations will be made employing the axisymmetric analog for three-dimensional boundary layers. Modified Newtonian pressures are used to illustrate the behavior of the maximum heating location. A more accurate pressure distribution could affect the precise location and level of heating. Results will be presented for several elliptic conic forebodies and heating-rate comparisons will be made to the method employed in Ref. 1.

For these calculations, a nondimensional time step of 0.01 was used. Typically, convergence of a single streamline was achieved in 5 to 10 iterations, or 0.0289 CPU s/point for a streamline and heating calculation on a Sun Microsystems SPARCstation 2.

Plane of Symmetry Surface Heating Rates

Previous work has shown evidence of maximum surface heating rates occurring away from the stagnation point on various blunted forebodies. A classical example of this phenomenon was demonstrated by Kemp et al.[17] on a flat-nosed body with rounded corners. This occurs because the maximum velocity gradient is at some point other than the stagnation point and is a result of geometry or angle of attack. Gnoffo,[18] using an upwind, perfect-gas relaxation algorithm, showed for the AFE vehicle[19] that maximum heating did not occur at the stagnation point. These results were substantiated by the experimental data of Micol[20] on the same vehicle. The forebody of this vehicle is defined by an ellipsoid and is described in detail in Ref. 19. To determine the effect of the forebody geometry on the stagnation region heating, laminar heat transfer calculations are made on various elliptic conics.

The controlling parameters in defining a particular elliptic conic are b_y, which defines the type of conic section in the plane of symmetry, and $\mathcal{C}$, the square of ratio of the principal axes in a cross-sectional plane, as shown in Fig. 1. All cases to be presented are investigated at a freestream Mach number of 10 and assume a perfect-gas equation of state.

Initially, a comparison is made to the previous method described in Ref. 1. As discussed earlier, inaccurate approximations were made when determining the initial conditions of the shooting technique. These inaccuracies caused oscillations or discontinuities in heating rates near the stagnation point, especially for nonspherical nose geometries. This effect and the improvements made by the present method are illustrated on a highly elliptic nose similar to that found on the AFE vehicle. The nose is defined by an ellipsoid with parameters $b_y = 4.0$ and $\mathcal{C} = 0.658$ as shown in Fig. 2.

In Fig. 3, the heat transfer rate, nondimensionalized by its value at the stagnation point, is plotted vs the nondimensional wetted surface distance measured from the nose point of the forebody. This case is for a 0 deg angle of attack. In comparison, we see that both methods compare very well away from the stagnation point. However, oscillations are produced at the stagnation point by the NHEAT code, whereas smoothly varying heating rates result from the present method. These effects can easily be seen in the expanded view of the stagnation region in Fig. 4.

Another noticeable phenomenon produced by both codes (not considering the oscillations of the NHEAT code) is that the location of maximum heating is away from the stagnation

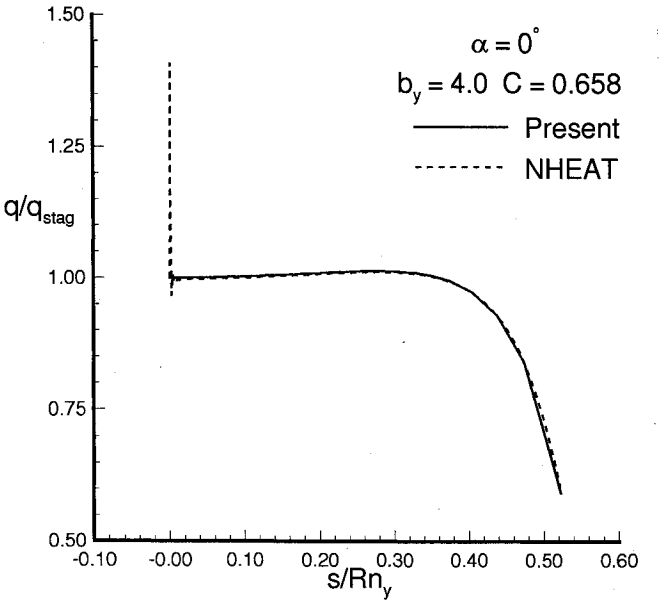

Fig. 3 Plane of symmetry heating comparison for AFE-like ellipsoid.

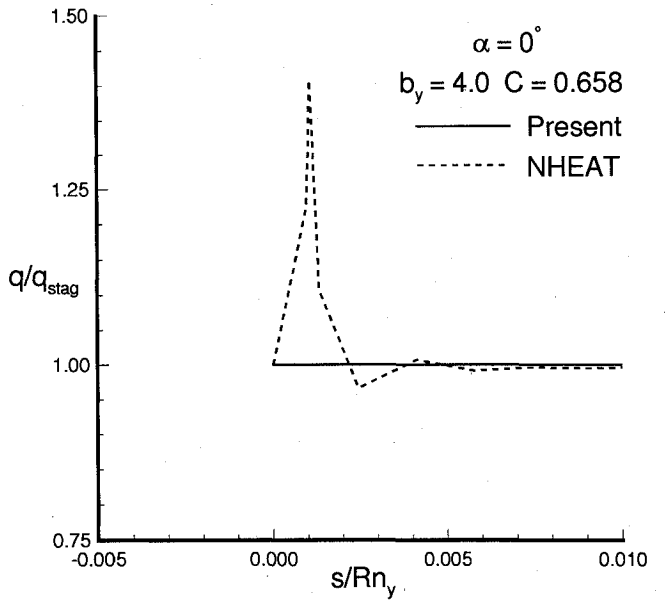

Fig. 4 Expanded view of plane of symmetry heating comparison for AFE-like ellipsoid.

point. The point of maximum heating occurs at an s/R_{n_y} of about 0.3. This effect was discussed earlier in this section in regard to the AFE vehicle. Since the nose is highly elliptic in the plane of symmetry, i.e., $b_y = 4.0$, the flat nose configuration of Ref. 17 is being approached. This occurrence of maximum heating away from the stagnation point for $\alpha = 0$ deg was seen for values of b_y greater than about 3.6 and is more pronounced for higher values. Subsequent cases will further illustrate this effect.

Next a parametric study is made to see the effect of the nose geometry on the position of the maximum heating rate. Each of the three conic sections, the ellipsoid, the paraboloid, and the hyperboloid, with the sphere being a special case of the ellipsoid, are investigated.

In Fig. 5, the ratio of the heating rate to that of a reference value is plotted vs the nondimensional wetted surface distance again measured from the nose point for the five different values of b_y examined. The reference heating value q_{ref} is for a sphere with a radius of unity. Several observations can now be made regarding the heating trends of elliptic conic forebodies. Initially the cross sectional ellipticity $\mathcal{C}$ is held constant at a value of 0.25 and the angle of attack is 20 deg. First, for values of the conic section parameter b_y equaling unity, a sphere in the plane of symmetry, maximum heating occurs at the stagnation point of the body. However, when the type of conic in the plane of symmetry is changed from unity, i.e., the spherical case, some interesting results are observed. For the case where b_y is greater than unity, it is observed that maximum heating on a blunt ellipsoid with $b_y = 2.0$ occurs aft of the stagnation point. This shape is similar to that of Fig. 2 but not as blunt. Maximum heating tends to occur at points where the curvature is rapidly changing because the maximum velocity gradient occurs there rather than the stagnation point. For this case, this region is aft of the stagnation point.

Next we see quite the opposite trend for an ellipsoid with b_y less than unity. For this ellipsoid where $b_y = 0.5$, the location of maximum heating lies between the stagnation point and the nose point. Again, this is the region of maximum curvature

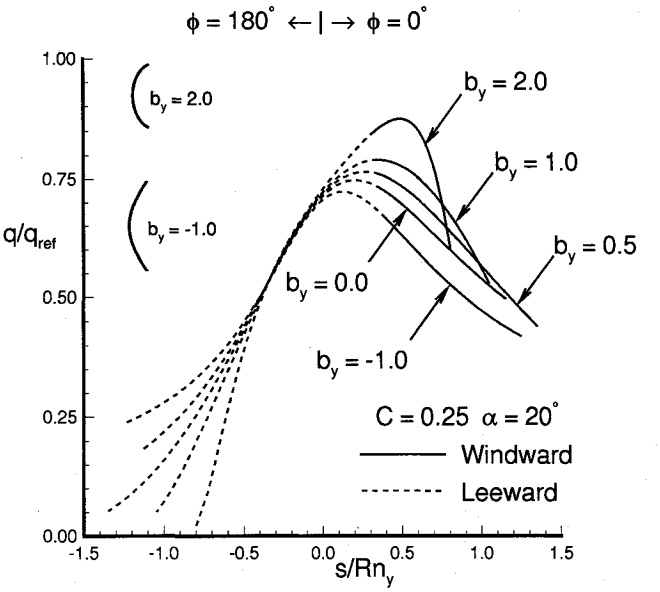

Fig. 5 Effect of conic section parameter b_y on the plane of symmetry heating.

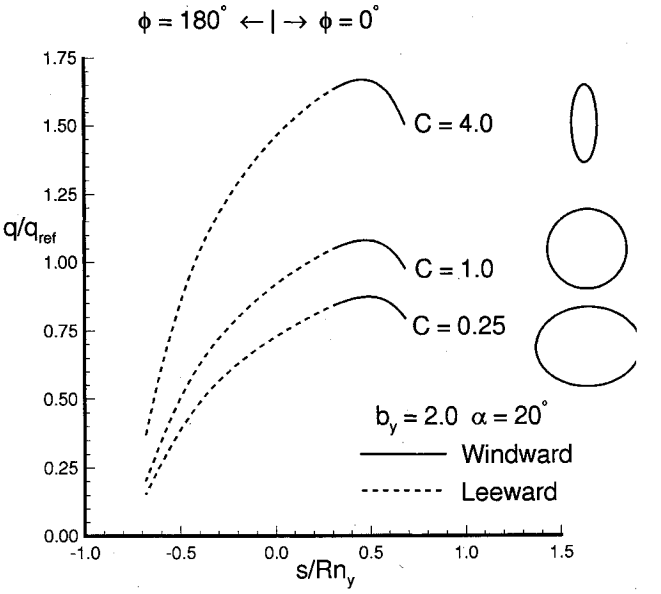

Fig. 6 Effect of cross-sectional ellipticity parameter $\mathcal{C}$ on the plane of symmetry heating.

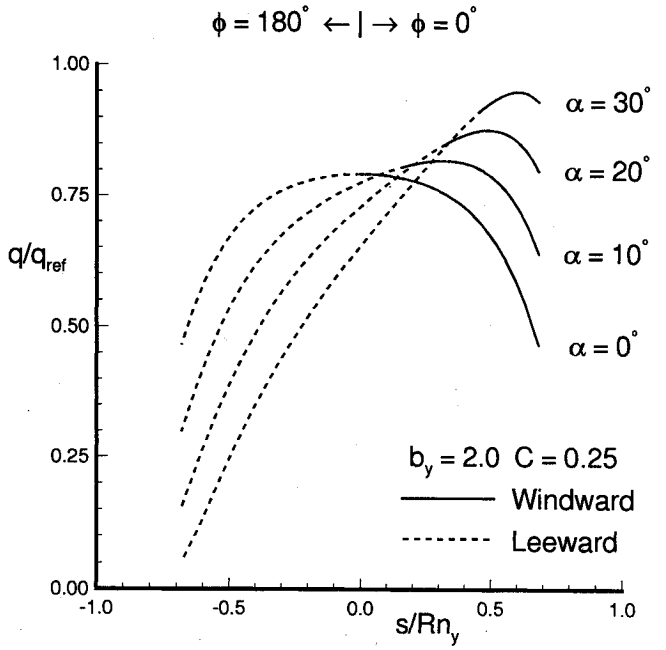

Fig. 7 Effect of angle of attack on the plane of symmetry heating.

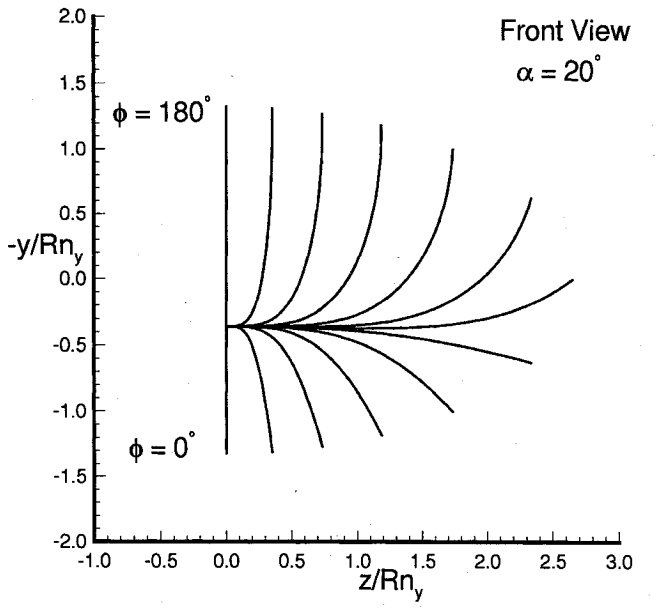

Fig. 8 Streamline geometry for ellipsoid with $b_y = 0.5$ and $\mathcal{C} = 0.25$.

for this body shape. However these effects are not exclusive to ellipsoids but can also be demonstrated for both the hyperboloid and the paraboloid, which both have b_y less than unity. Like the ellipsoid with $b_y = 0.5$, it is seen in Fig. 5 that the point of maximum heating occurs between the nose point and the stagnation point for both the paraboloid ($b_y = 0$) and the hyperboloid ($b_y = -1.0$).

The effects of cross-sectional ellipticity and angle of attack are considered next. In Fig. 6, an ellipsoid with $b_y = 2.0$ at an angle of attack of 20 deg is investigated for three different cross sections: $\mathcal{C} = 0.25$, 1.0 (axisymmetric), and 4.0. Values of $\mathcal{C}$ less than unity but positive represent bodies with flat cross sections whereas thin bodies occur for $\mathcal{C}$ greater than unity. As expected, the point of maximum heating occurs aft of the stagnation point for this case where b_y is greater than unity and the overall heating increases with increasing $\mathcal{C}$. An unexpected observation from this figure is that the location of the point of maximum heating seems to be independent of the

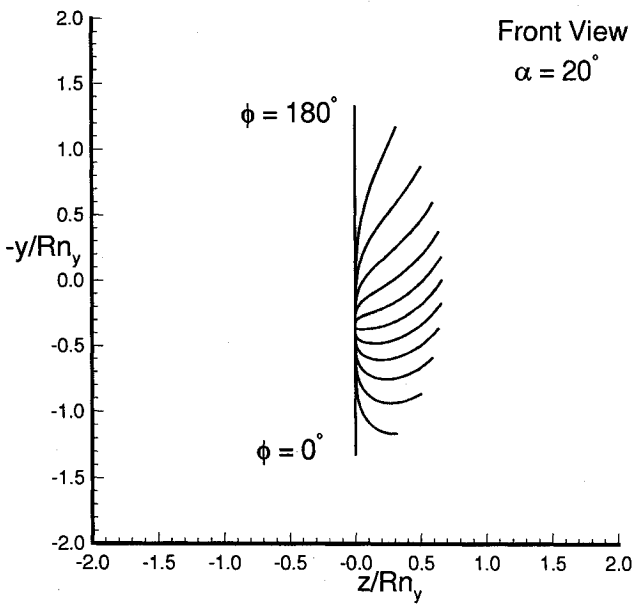

Fig. 9 Streamline geometry for ellipsoid with $b_y = 0.5$ and $\mathcal{C} = 4.0$.

elliptic cross-sectional parameter $\mathcal{C}$. The same effect was observed to occur for slender ellipsoids as well as hyperboloids and paraboloids.

For an ellipsoid with $b_y = 2.0$ and $\mathcal{C} = 0.25$, the effect of angle of attack on the surface heating rates is investigated in Fig. 7. The plane of symmetry heating is plotted for a range of angles of attack. It is observed that for the 0-deg angle-of-attack case, the nose point, stagnation point, and point of maximum heating are all coincident. However, as already demonstrated, this effect is not necessarily the case for blunter geometries. Finally, as the angle of attack is increased for this geometry, the point of maximum heating occurs aft of the stagnation point, as noted in earlier cases.

Three-Dimensional Streamline Geometry

The effect of cross-sectional ellipticity on the streamline geometry is investigated on an ellipsoid with $b_y = 0.5$ and two different cross sections at an angle of attack of 20 deg. First a relatively flat forebody shape with $\mathcal{C} = 0.25$ is demonstrated in Fig. 8 for 20-deg angle of attack. The streamlines leave the stagnation region in a much different manner than the sphere case where the resulting streamlines emanate radially from the stagnation point and form great circles around the sphere. All streamlines tend to approach the stagnation point asymptotically along the $\beta = 90$ deg streamline once in the stagnation region. It is seen that for this angle-of-attack case, the streamlines tend to group toward the respective planes of symmetry in the downstream region.

However, for the case of a relatively thin body where $\mathcal{C} = 4.0$, the streamline patterns have a different character. It is seen in Fig. 9 that the streamlines tend to approach the stagnation point from either of the planes of symmetry when in the stagnation region and not along the same line as in the preceding case. The opposite trend is also seen in the downstream region as the streamlines are much more evenly spaced and tend to group away from the planes of symmetry.

Conclusions

As a result of the investigations described in this paper, the following conclusions were drawn:

1) Previous problems of integrating the streamline equations through the nose point and in the stagnation region have been eliminated by the use of Cartesian coordinates and time as the independent variable of integration. The streamline that passes through a particular downstream point can be computed by this new technique. The use of time as the indepen-

dent variable of integration magnifies the computational domain of the stagnation region and eliminates the need for using small step sizes associated with a spatial integration to achieve desired accuracy in the stagnation region.

2) The location of maximum heating is affected by the type of conic section in the plane of symmetry and the angle of attack. Cross-sectional ellipticity affects the level of the heating but has little or no effect on the location of maximum heating. For the conic section parameter b_y greater than unity, maximum heating occurs aft of the stagnation point whereas the point of maximum heating lies between the stagnation point and the nose point for b_y less than unity for cases at angle of attack. However, maximum heating occurred at the stagnation point for $b_y = 1.0$.

3) The method developed herein can also be used in conjunction with other codes which calculate surface pressures or the inviscid flowfield.

Acknowledgments

This work is supported in part by the following grants: the Hypersonic Aerodynamics Training and Research Grant NAGW-1072 funded jointly by NASA, Air Force Office of Scientific Research and Office of Naval Research; and NASA Langley Research Center Cooperative Agreement NCC1-100 with the Aerothermodynamics Branch of the Space Systems Division. The authors would like to extend special thanks to F. McNeil Cheatwood of Vigyan Research Associates Inc., and Christopher J. Riley, H. Harris Hamilton II, and Peter A. Gnoffo of NASA Langley Research Center for their many helpful discussions. In addition, the authors would also like to extend their gratitude to the members of the Aerothermodynamics Branch at NASA Langley Research Center for providing computer resources and technical advice.

References

[1]Cooke, J. C., "An Axially Symmetric Analogue for General Three-Dimensional Boundary Layers," British Ministry of Aviation, R&M. No. 3220, Aeronautical Research Council TR, London, June 1961.

[2]DeJarnette, F. R., and Hamilton, H. H., II, "Inviscid Surface Streamlines and Heat Transfer on Shuttle-Type Configurations," *Journal of Spacecraft and Rockets,* Vol. 10, No. 5, 1973, pp. 314–321.

[3]Leigh, D. C., and Ross, B. B., " Surface Geometry of Three-Dimensional Inviscid Hypersonic Flows," *AIAA Journal,* Vol. 7, No. 1, 1969, pp. 123–129.

[4]Berman, R. J., "Method for Prediction of Aerodynamic Coefficients for Blunted Sphere-Cones at Angle of Attack," Re-entry Systems Div., General Electric Co., AFM 123, June 1961.

[5]Vaglio-Laurin, R., "Laminar Heat Transfer on Three-Dimensional Blunt Nosed Bodies in Hypersonic Flow," *ARS Journal,* Vol. 29, No. 2, 1959, pp. 123–129.

[6]Vollmers, H., "Integration of Streamlines from Measured Static Pressure Fields on a Surface," *AIAA Journal,* Vol. 20, No. 10, 1982, pp. 1459–1460.

[7]Hamilton, H. H., II, DeJarnette, F. R., and Weilmuenster, K. J., "Application of Axisymmetric Analogue for Calculating Heating Rates in Three-Dimensional Flows," AIAA Paper 85-0245, Jan. 1985.

[8]Weilmuenster, K. J., and Hamilton, H. H., II, "Calculation of Inviscid Flow Over Shuttle-Like Vehicles at High Angles of Attack and Comparisons with Experimental Data," NASA TP 2103, May 1983.

[9]Rakich, J. V., and Mateer, G. G., "Calculation of Metric Coefficients for Streamline Coordinates," *AIAA Journal,* Vol. 10, No. 11, 1972, pp. 1540–1583.

[10]Rakich, J. V., and Pegot, E. B., "Flow Field and Heating on the Windward Side of the Space Shuttle Orbiter," NASA SP 347, March 1975.

[11]Rakich, J. V., and Lanfranco, M. J., "Numerical Computation of Space Shuttle Heating and Surface Streamlines," AIAA Paper 76-464, July 1976.

[12]Fannelop, T. K., "A Method of Solving Three-Dimensional Laminar Boundary-Layer Equations with Application to a Lifting Re-Entry Body," *AIAA Journal,* Vol. 6, No. 6, 1968, pp. 1075–1084.

[13]Hassan, B., "Calculation of Streamlines and Metrics from Pressure Distributions for Predicting Heating Rates," M.S. Thesis, Dept. of Mechanical and Aerospace Engineering, North Carolina State Univ., Raleigh, NC, Oct. 1990.

[14]Love, E. S., Woods, W. C., Rainey R. W., and Ashby, G. C. Jr., "Some Topics in Hypersonic Body Shaping," AIAA Paper 69-181, Jan. 1969.

[15]Blottner, F. G., "Introduction to Computational Techniques for Boundary Layers," Sandia Lab. Release SAND 79-0893, Albuquerque, NM, Sept. 1979.

[16]Anderson, D. A., Tannehill, J. C., and Pletcher, R. H., *Computational Fluid Mechanics and Heat Transfer,* McGraw-Hill, New York, 1984, pp. 551–557.

[17]Kemp, N. H., Rose, P. H., and Detra, R. W., "Laminar Heat Transfer Around Blunted Bodies in Dissociated Air," *Journal of the Aerospace Sciences,* Vol. 26, No. 7, 1959, pp. 421–430.

[18]Gnoffo, P. A., "An Upwind-Biased, Point-Implicit Relaxation Algorithm for Viscous, Compressible Perfect-Gas Flows," NASA TP 2953, Feb. 1990.

[19]Cheatwood, F. M., DeJarnette, F. R., and Hamilton, H. H., II, "Geometrical Description for a Proposed Aeroassist Flight Experimental Vehicle," NASA TM 87714, July 1986.

[20]Micol, J. R., "Experimental and Predicted Pressure and Heating Distributions for an Aeroassist Flight Experiment Vehicle in Air at Mach 10," AIAA Paper 89-1731, June 1989.

Gerald T. Chrusciel
Associate Editor